JOURNAL OF THE AMERICAN CHEMICAL SOCIETY

Article

Intramolecular Charge Transfer in 4-Aminobenzonitriles Does Not Necessarily Need the Twist

Isabel Gmez, Mar Reguero, Martial Boggio-Pasqua, and Michael A. Robb

J. Am. Chem. Soc., **2005**, 127 (19), 7119-7129• DOI: 10.1021/ja042413w • Publication Date (Web): 26 April 2005

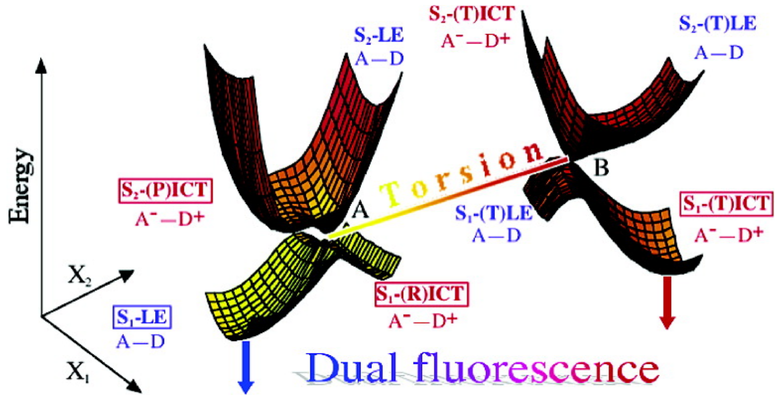

Journal of the American Chemical Society is published by the American Chemical Society. 1155 Sixteenth Street N.W., Washington, DC 20036

J|A|C|S
ARTICLES

Intramolecular Charge Transfer in 4-Aminobenzonitriles Does Not Necessarily Need the Twist

Isabel Gómez,[†] Mar Reguero,[†] Martial Boggio-Pasqua,[‡] and Michael A. Robb[*,‡]

Contribution from the Departament de Química Física i Inorgànica, Pl. Imperial Tarraco 1,
43005 Tarragona, Spain, and Department of Chemistry, Imperial College London, South
Kensington Campus, SW7 2AZ, UK

Received December 17, 2004; E-mail: mike.robb@imperial.ac.uk

Abstract: In electron donor/acceptor species such as 4-(dimethylamino)benzonitrile (DMABN), the excitation to the S_2 state is followed by internal conversion to the locally excited (LE) state. Dual fluorescence then becomes possible from both the LE and the twisted intramolecular charge-transfer (TICT) states. A detailed mechanism for the ICT of DMABN and 4-aminobenzonitrile (ABN) is presented in this work. The two emitting S_1 species are adiabatically linked along the amino torsion reaction coordinate. However, the S_2/S_1 CT-LE radiationless decay occurs via an extended conical intersection "seam" that runs almost parallel to this torsional coordinate. At the lowest energy point on this conical intersection seam, the amino group is untwisted; however, the seam is accessible for a large range of torsional angles. Thus, the S_1 LE-TICT equilibration and dual fluorescence will be controlled by (a) the S_1 torsional reaction path and (b) the position along the amino group twist coordinate where the S_2/S_1 CT-LE radiationless decay occurs. For DMABN, population of LE and TICT can occur because the two species have similar stabilities. However, in ABN, the equilibrium lies in favor of LE, as a TICT state was found at much higher energy with a low reaction barrier toward LE. This explains why dual fluorescence cannot be observed in ABN. The $S_1 \rightarrow S_0$ deactivation channel accessible from the LE state was also studied.

Introduction

4-(Dimethylamino)benzonitrile (DMABN) is a prototype system for molecular dual fluorescence first discussed by Lippert.[1] Upon excitation in the near UV using a solvent of suitable polarity, the emission spectrum displays two fluorescence bands: one with the usual small Stokes shift (assigned to a benzenoid $\pi-\pi^*$ excited state, the ^1L_b-type state, or locally excited (LE) state), and a second band, with a large red-shift (attributed to the emission from a highly polar intramolecular charge-transfer (ICT) state, the ^1L_a-type state). Dual fluorescence depends on the relative energy of the two states, which can be fine-tuned with the polarity of the solvent. As a consequence, the intensity of the anomalous fluorescence increases to the detriment of the normal emission as the polarity of the medium increases. In the gas phase, no fluorescence is observed from the ICT state because it is higher than the LE state (for a review, see ref 2). The mechanism behind such a phenomenon is highly controversial and has been the subject of many experimental[1,3−26] and theoretical studies.[27−50] The central issues relate to (a) the molecular and electronic structures of the emitting ICT species, (b) the nature of the adiabatic reaction pathway that connects the LE species to the ICT emitting state, and (c) the nature of

---

[†] Departament de Química Física i Inorgànica.

[‡] Imperial College London.

(1) Lippert, E.; Lüder, W.; Boos, H. In *Advances in Molecular Spectroscopy*; Mangini, A., Ed.; Pergamon: Oxford, 1962; pp 443−457.

(2) Grabowski, Z. R.; Rotkiewicz, K.; Rettig, W. *Chem. Rev.* **2003**, *103*, 3899−4031.

(3) Rettig, W.; Bliss, B.; Dirnberger, K. *Chem. Phys. Lett.* **1999**, *305*, 8−14.

(4) Lippert, E.; Lüder, W.; Moll, F.; Nägele, W.; Boos, H.; Prigge, H.; Seibold-Blankenstein, I. *Angew. Chem.* **1961**, *73*, 695−706.

(5) Rotkiewicz, K.; Grellmann, K. H.; Grabowski, Z. R. *Chem. Phys. Lett.* **1973**, *19*, 315−318.

(6) Rotkiewicz, K.; Grellmann, K. H.; Grabowski, Z. R. *Chem. Phys. Lett.* **1973**, *21*, 212.

(7) Rettig, W. Angew. *Chem., Int. Ed. Engl.* **1986**, *25*, 971−988.

(8) Lippert, E.; Rettig, W.; Bonacic-Koutecky, V.; Heisel, F.; Miehé, J. A. *Adv. Chem. Phys.* **1987**, *68*, 1−173 and references therein.

(9) Rettig, W. In *Topics in Current Chemistry, Electron-Transfer I*; Mattay, J., Ed.; Springer: Berlin, 1994; Vol. 169, pp 253−299.

(10) Leinhos, U.; Kühnle, W.; Zachariasse, K. A. *J. Phys. Chem.* **1991**, *95*, 2013−2021.

(11) Schuddeboom, W.; Jonker, S. A.; Warman, J. H.; Leinhos, U.; Kühnle, W.; Zachariasse, K. A. *J. Phys. Chem.* **1992**, *96*, 10809−10819.

(12) Zachariasse, K. A.; von der Haar, T.; Hebecker, A.; Leinhos, U.; Kühnle, W. *Pure Appl. Chem.* **1993**, *65*, 1745−1750.

(13) von der Haar, T.; Hebecker, A.; Il'ichev, Y. V.; Jiang, Y.-B.; Kühnle, W.; Zachariasse, K. A. *Recl. Trav. Chim. Pays-Bas* **1995**, *114*, 430.

(14) Zachariasse, K. A.; Grobys, M.; von der Haar, T.; Hebecker, A.; Il'ichev, Y. V.; Jiang, Y.-B.; Morawski, O.; Kühnle, W. *J. Photochem. Photobiol., A: Chem.* **1996**, *102*, 59−70.

(15) Il'ichev, Y. V.; Kühnle, W.; Zachariasse, K. A. *J. Phys. Chem. A* **1998**, *102*, 5670−5680.

(16) Zachariasse, K. A. *Chem. Phys. Lett.* **2000**, *320*, 8−13.

(17) Demeter, A.; Druzhinin, S.; George, M.; Haselbach, E., Roulin, J.-L.; Zachariasse, K. A. *Chem. Phys. Lett.* **2000**, *323*, 351−360.

(18) Changenet, P.; Plaza, P.; Martin, M. M.; Meyer, Y. H. *J. Phys. Chem. A* **1997**, *101*, 8186−8194.

(19) Su, S.-G.; Simon, J. D. *J. Chem. Phys.* **1988**, *89*, 908−919.

(20) Okamoto, H.; Inishi, H.; Nakamura, Y.; Kohtani, S.; Nakagaki, R. *J. Phys. Chem. A* **2001**, *105*, 4182−4188.

(21) Kwok, W. M.; Ma, C.; Matousek, P.; Parker, A. W.; Phillips, D.; Toner, W. T.; Towrie, M.; Umapathy, S. *J. Phys. Chem. A* **2001**, *105*, 984−990.

(22) Ma, C.; Kwok, W. M.; Matousek, P.; Parker, A. W.; Phillips, D.; Toner, W. T.; Towrie, M. *J. Phys. Chem. A* **2002**, *106*, 3294−3305.

(23) Techert, S.; Zachariasse, K. A. *J. Am. Chem. Soc.* **2004**, *126*, 5593−5600.

(24) Zachariasse, K. A.; Druzhinin, S. I.; Bosch, W.; Machinek, R. *J. Am. Chem. Soc.* **2004**, *126*, 1705−1715.

(25) Yoshihara, T.; Druzhinin, S. I.; Zachariasse, K. A. *J. Am. Chem. Soc.* **2004**, *126*, 8535−8539.

(26) Fuss, W.; Pushpa, K. K.; Rettig, W.; Schmid, W. E.; Trushin, S. A. *Photochem. Photobiol. Sci.* **2002**, *1*, 255−262.

10.1021/ja042413w CCC: $30.25 © 2005 American Chemical Society

the nonadiabatic reaction path (recently documented by Fuβ[26]) via a conical intersection (CI), which connects the FC structure on S_2 to the LE and ICT species that emit from S_1.

Our discussion of the TICT problem requires some definitions and clarifications of basic mechanistic terms as a prelude. In general, mechanistic information is usually conveyed as a sequence of structures (geometries) that connect initial and final geometries along some reaction path. Yet excited-state reaction paths can span several potential energy surfaces so one also needs to add a state label (S_0, S_1, etc.) to such geometries. The transition from the reaction path on one state to the reaction path on another state occurs at conical intersections,[51,52] and the geometry associated with such surface crossings is a central mechanistic element for excited-state dynamics. Thus, in this paper, for any given geometry, we will label the structure with (a) the state label (S_0, S_1, S_2) and (b) the geometry (e.g., planar P, rehybridized R, and twisted T). For example, we will denote a planar ICT structure on S_2 as S_2-(P)ICT. This clarification of the nomenclature is necessary because the nomenclature used by experimentalists does not distinguish between a planar ICT structure on S_2 (which we shall call S_2-(P)ICT) and a planar CT structure on S_1 (which we shall call S_1-(P)ICT). Emission might occur from the lowest energy structure S_1-(P)ICT but obviously not from S_2-(P)ICT, so the notation PICT on its own is ambiguous.

The electronic structure can be rigorously calculated from an analysis of the computed excited-state wave function. The language of the valence bond (VB) theory is particularly convenient, and we will use this language to describe the electronic structure. Thus, a charge-transfer (ICT) state has a distinct electronic (i.e., VB) structure that is different from that of a locally excited state (LE) (see Scheme 1). We shall refer to zwitterionic VB structures, such as III or IV in Scheme 1, as charge-transfer structures. In contrast, we use the name "dot-dot" to denote covalent structures such as I and II.

Scheme 1

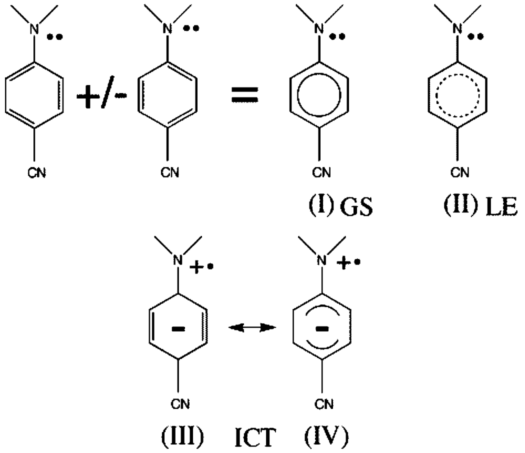

We begin with a discussion of the molecular and electronic structures of the emitting ICT species. Four different types of molecular structures have been proposed for the emitting ICT species of DMABN. In the twisted ICT (T)ICT model,[5,6] the amino group is in a perpendicular position relative to the benzene ring. A planar ICT (P)ICT structure has been suggested by Zachariasse[10−15,23,24] in which the amino group lies in the benzene plane. The wagged ICT (W)ICT suggested by Zachariasse[11,12,46] involves a rehybridization from planar sp^2 to pyramidal sp^3 of the amino nitrogen. Finally, the rehybridized ICT (R)ICT[29−31] involves a rehybridization of the cyano carbon atom from sp to sp^2 entailing a bent cyano bond.

The nature and magnitude of the electronic coupling between the electron donor (amino group) and the electron acceptor (benzonotrile moiety) parts requires some discussion and clarification. It is often assumed that the system is decoupled in the twisted conformation because of the zero overlap of the orbitals involved, leading to an increased charge separation in the TICT state. However, in the planar conformation, the amino and benzonitrile moieties are assumed to be strongly coupled in a PICT state. Thus, the usual assumption is that the N-phenyl bond has a single-bond character in TICT, while it has a double-bond character in PICT.[15,16] Experimentally, from picosecond infrared[20] and resonance Raman[21] measurements, and calculations of IR frequencies,[36] it was concluded that the N-phenyl bond has a single-bond character in the ICT state, which would support the TICT model. Theoretical computations[37] suggest that the ICT state has a strong quinoidal character in the phenyl moiety (which would favor the PICT structure), and a decrease of quinoidality would be expected when the amino group was decoupled from the rest of the molecule in TICT. In their calculations, Zilberg and Haas[37] could only find a planar quinoid ICT state on the S_2 surface of ABN and no quinoidal TICT structure. (Note that these authors also present results on PBN, a pyrrolo-derivative of DMABN for which the ICT state has a different structure.) However, several calculations[29,36,38,39] have found a quinoidal TICT state on S_1, including the most recent correlated CC2 (coupled-cluster singles and doubles) calculations by Köhn.[39] Thus, the twisted conformation of the amino group and the quinoidality of the phenyl ring may not be as contradictory as first thought. However, as we shall show subsequently, the intrinsic electronic coupling (as manifested

---

(27) Sudholt, W.; Sobolewski, A. L.; Domcke, W. *Chem. Phys.* **1999**, *250*, 9−18 and references therein.
(28) Serrano-Andrés, L.; Merchán, M.; Roos, B. O.; Lindh, R. *J. Am. Chem. Soc.* **1995**, *117*, 3189−3204.
(29) Sobolewski, A. L.; Domcke, W. *Chem. Phys. Lett.* **1996**, *259*, 119−127.
(30) Sobolewski, A. L.; Domcke, W. *Chem. Phys. Lett.* **1996**, *250*, 428−436.
(31) Sobolewski, A. L.; Sudholt, W.; Domcke, W. *J. Phys. Chem. A* **1998**, *102*, 2716−2722.
(32) Lommatzsch, U.; Brutschy, B. *Chem. Phys.* **1998**, *234*, 35−57.
(33) Parusel, A. B. J.; Köhler, G.; Grimme, S. *J. Phys. Chem. A* **1998**, *102*, 6297−6306.
(34) Parusel, A. B. J.; Köhler, G.; Nooijen, M. *J. Phys. Chem. A* **1999**, *103*, 4056−4064.
(35) Parusel, A. B. J.; Rettig, W.; Sudholt, W. *J. Phys. Chem. A* **2002**, *106*, 804−815.
(36) Dreyer, J.; Kummrow A. *J. Am. Chem. Soc.* **2000**, *122*, 2577−2585.
(37) Zilberg, S.; Haas, Y. *J. Phys. Chem. A* **2002**, *106*, 1−11.
(38) Rappoport, D.; Furche, F. *J. Am. Chem. Soc.* **2004**, *126*, 1277−1284.
(39) Köhn, A.; Hättig, C. *J. Am. Chem. Soc.* **2004**, *126*, 7399−7410.
(40) Gedeck, P.; Schneider, S. *J. Photochem. Photobiol., A: Chem.* **1997**, *105*, 165−181 and references therein.
(41) Moro, G. J.; Nordio, P. L.; Polimeno, A. *Mol. Phys.* **1989**, *68*, 1131−1141.
(42) Kato, S.; Amatatsu, Y. *J. Chem. Phys.* **1990**, *92*, 7241−7257.
(43) Fonseca, T.; Kim, H. J.; Hynes, J. T. *J. Mol. Liq.* **1994**, *60*, 161−200.
(44) Fonseca, T.; Kim, H. J.; Hynes, J. T. *J. Photochem. Photobiol., A: Chem.* **1994**, *82*, 67−79.
(45) Broo, A.; Zerner, M. C. *Theor. Chim. Acta* **1995**, *90*, 383−395.
(46) Gorse, A.-D.; Pesquer, M. *J. Phys. Chem.* **1995**, *99*, 4039−4049.
(47) Soujanya, T.; Saroja, G.; Samanta, A. *Chem. Phys. Lett.* **1995**, *236*, 503−509.
(48) Hayashi, S.; Ando, K.; Kato, S. *J. Phys. Chem.* **1995**, *99*, 955−964.
(49) Kim, H. J.; Hynes, J. T. *J. Photochem. Photobiol., A: Chem.* **1997**, *105*, 337−343.
(50) Mennucci, B.; Toniolo, A.; Tomasi, J. *J. Am. Chem. Soc.* **2000**, *122*, 10621−10630.
(51) (a) Michl, J.; Klessinger, M. *Excited States and Photochemistry of Organic Molecules*; VCH: New York, 1995. (b) Michl, J.; Bonacic-Koutecky, V. *Electronic Aspects of Organic Photochemistry*; Wiley: New York, 1990.
(52) Klessinger, M. *Angew. Chem., Int. Ed. Engl.* **1995**, *34*, 549−551.

in the VB structure) between the amino group and the benzene ring is large in both PICT and TICT structures. However, in the TICT structure, the overlap is zero so this coupling cannot stabilize the electronic structure.

The nature of the adiabatic reaction pathway, which connects the S_1 LE species to the S_1 ICT emitting state, has been discussed extensively in the experimental and theoretical literature. Experiments by Zachariasse[10−15,17,23−25] have focused on this adiabatic reaction path. The S_1 reaction coordinate has often been postulated to involve the twist of the amino group relative to the benzene ring. This is the origin of the "TICT mechanism". Nonresonant multiphoton ionization experiments support this reaction coordinate.[26,53] However, the planarization of the amino group coupled with a quinoidization coordinate was also suggested as an alternative reaction coordinate.[10−15,23−25] Moreover, Köhn[39] suggested this coordinate could be a possible decay path after initial vertical excitation to S_2. For this model, the term "planar intramolecular charge transfer" was coined. This model has been supported by a recent experiment on 4-(diisopropylamino)benzonitrile (related to DMABN) in the crystal phase.[23] Another experiment revealing dual fluorescence in a planar rigidized aminobenzonitrile also casts doubts on the TICT mechanism.[24]

The nature of the nonadiabatic reaction path, which connects the FC structure on S_2 to the LE and ICT species on S_1, which subsequently emit from S_1 is a distinct mechanistic issue. The computations of Serrano-Andrés,[28] as shown by oscillator strength values, demonstrate that the S_2 L_a-type state should be considered as the initially promoted state, although it is not the lowest excited state in the Franck−Condon region (the ^1L_b-type state is lower in energy). Thus, the S_2 L_a-type state carries most of the energy following absorption because of the allowed Franck−Condon character. This result confirms the previous experiments on polarization measurements.[1,4] In a recent experiment by Fu*β*,[26] the initial reaction path, which evolves on the S_2 L_a-type state, was observed directly. The experiments of Fu*β* show that S_2 evolution is followed by an ultrafast internal conversion (radiationless decay) to S_1 with subsequent evolution on S_1 to the LE and ICT minimum energy structures. Therefore, the initial part of the reaction path following light absorption must be nonadiabatic. The adiabatic reaction channel (connecting the LE and ICT emitting species on S_1) is then subsequently populated on S_1. Thus, Fu*β* claims that ICT and LE are formed from S_n via the CI in a branching process. As we shall discuss subsequently, observation of ICT emission is controlled by the ICT-LE barrier. Consequently, two ICT reaction paths need to be characterized theoretically: (a) the nonadiabatic S_2/S_1 reaction path leading through the funnel (conical intersection seam) and (b) the subsequent adiabatic S_1 reaction path where equilibration takes place. This also raises the question as to the geometry on the CI where the S_1 adiabatic reaction channel is entered from S_2. As we shall discuss subsequently, the presence of an extended conical intersection seam means that S_1 can be populated over a range of twist and pyramidalization angles.

Theoretical contributions have also given some insight as to the nature of the ICT reaction coordinate. As a general rule, most theoretical studies point toward the amino group twist as the reaction coordinate along which a state switch occurs (either at conical intersection or at an avoided crossing giving rise to a transition state) between the LE and ICT states and leads to a low-lying TICT state.[28,31,33,34,36,39,49,50] However, recent high-level ab initio calculations have suggested that those two states can cross along the pyramidalization of the ring carbon atom to which the dimethylamino group is attached, without the twisting motion.[39] Thus, this pyramidalization coordinate constitutes another possible decay path after initial vertical excitation to the L_a-type state.

Scheme 2

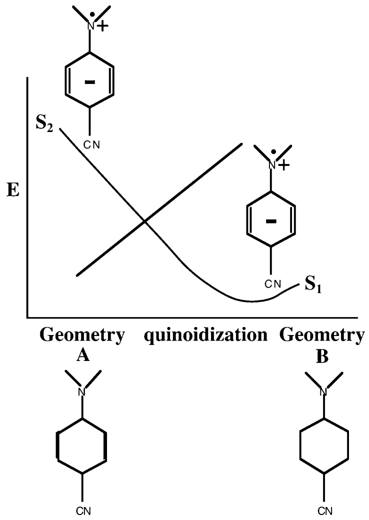

Unfortunately, in many theoretical studies,[28,34,39,50] the computations have been based either on rigid or on relaxed (with geometry optimization at each point) scans of the excited-state surfaces along the torsion coordinate. Thus, the separation of adiabatic and nonadiabatic processes is not clear, and one cannot make any conclusion about the coordinate along which the nonadiabatic decay is going to take place. For this, one needs information about the actual conical intersection and the two degeneracy-lifting coordinates so important in the understanding of the dynamics of nonadiabatic processes.

It is clear the connection between molecular structure, electronic (VB) structure, and the nature of the adiabatic and nonadiabatic pathways between dot-dot and ICT structures are the central issues in the TICT controversy. Thus, in the next section, we give a brief introduction of the concepts required to unify this area.

Conceptual Development: The Nature of the Extended Conical Intersection Seam

The relationship between the VB structure and geometry is important but subtle because the same VB structure can be associated with distinct geometric structures on two different excited state surfaces. This idea is particularly relevant near a conical intersection and is illustrated in Scheme 2. For a given geometry (geometry A in Scheme 2), the electronic structure corresponding to VB structure III (Scheme 1) lies on S_2. On changing the geometry A to geometry B (Scheme 2), one passes through a conical intersection (diabatically), and at geometry B the S_1 surface has a minimum with the electronic structure III. In fact, a circuit of geometries (in the space of the degeneracy-lifting coordinates) around a conical intersection

---

(53) Fu*β*, W.; Rettig, W.; Schmid, W. E.; Trushin, S. A.; Yatsuhashi, T. *Faraday Discuss.* **2004**, *127*, 23−33.

Scheme 3

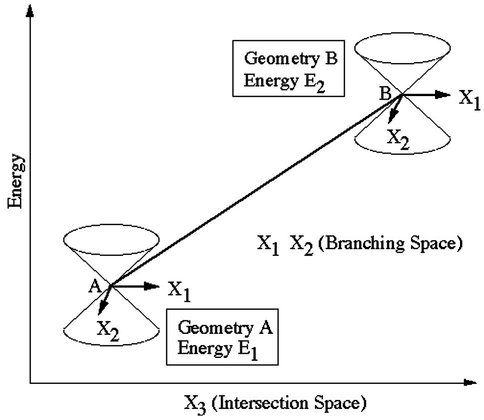

Scheme 4

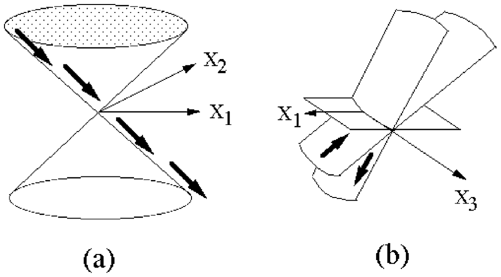

point must pass through a same VB structure (once on the upper state and once on the lower state).[54]

The last conceptual point that needs to be focused on at this stage concerns the conical intersection itself (Scheme 3). The surface crossing is characterized by two degeneracy-lifting geometric coordinates X_1 and X_2 spanning the "branching space". In these coordinates, the potential energy surfaces appear as a double cone. As the geometry is changed through a third coordinate X_3 (from the "intersection space"), which lies outside the (X_1, X_2) space, the degeneracy remains. This is shown in Scheme 3. At geometry A, the conical intersection structure has energy E_1. At geometry B, the two states are still degenerate; however, the energy changes to E_2. Further, the detailed shape of the two intersecting surfaces will change at points A and B, and this has important chemical consequences that we shall subsequently discuss. The "line" joining points A and B is the "seam" of the conical intersection. This can be more easily visualized when the energy is plotted in one coordinate from the branching space X_1 and one coordinate from the intersection space X_3 (Scheme 4b). One then sees a "seam" of intersection in this three-dimensional sub-space. A reaction path that characterizes chemical change can have various orientations with respect to the branching space. If the reaction path lies in the space (X_1, X_2) (arrows in Scheme 4a), then the passage through the cone is like sand in a funnel. On the other hand, if the reaction path lies orthogonal to (X_1, X_2) (arrows in Scheme 4b), then the crossing seam is entered via motion orthogonal to the reaction path.

With this conceptual development in hand, we can now summarize the central mechanistic questions related to the TICT problem. Charge transfer can obviously only occur, with no change in geometric structure, in a radiative process, such as excitation from the ground state to a ICT state with electronic structure III in Scheme 1. In the TICT problem, we are mainly concerned with the problem where ICT occurs as a radiationless process. In this case, one must have a geometrical change with a concomitant change in the electronic structure from a dot-dot structure such as II to a CT structure such as III in Scheme 1 (i.e., the ICT process involves a change in VB structure). Thus, the ICT process can occur as a nonadiabatic process, and our theoretical work involves a study of the CI line associated with decay from $L_a(S_2)$ to $L_b(S_1)$ illustrated in Scheme 3. Alternatively ICT occurs as an adiabatic process and one must characterize the geometry, and the VB structures of the LE and ICT minima on S_1 associated with dual fluorescence. Finally, the relationship between these two processes must be established. Additionally, in an aside, we will discuss the observed decrease of fluorescence yield from the LE state with temperature.[55]

Computational Details

The different electronic states of ABN and DMABN have been studied with complete active space self-consistent field (CASSCF)[56] using a 6-31G(d) basis set.[57] The (12e,11o) CASSCF includes the benzene π orbitals, the amino nitrogen lone pair, and the four cyano π orbitals. Full geometry optimizations were performed without any symmetry constraint. Numerical frequency calculations were calculated for ABN to determine the nature of the stationary points. Intrinsic reaction coordinates (IRCs) were also computed to determine the pathways linking the critical structures (stationary points and CI).

The physically important part of the dynamic correlation, which is crucial in the description of polar electronic states, was included using restricted active space self-consistent field[58] (RASSCF). Eighteen electrons were distributed in 18 orbitals, with the orbital spaces RAS1, RAS2, and RAS3 containing seven, four, and seven orbitals, respectively. Single and double excitations were allowed from RAS1, and no more than two electrons were allowed in RAS3 in all configuration state functions. The orbitals were selected using a simplified iterative natural orbital scheme. RASSCF permits full geometry optimization, and the energetics can be comparable with multireference configuration interaction (MRCI) and multiconfigurational second-order perturbation theory (CASPT2) in some cases.[59] ABN geometries were reoptimized at this level, and CASPT2 energetics[60] were also computed for comparison at both the CASSCF and the RASSCF optimized geometries (Table 1). Solvent effects have not been included in this study, but calculations in vacuo are sufficient to provide reliable mechanistic information.

Conical intersections were optimized using the algorithm described in ref 61. State-averaged orbitals were used, and the orbital rotation derivative correction (which is usually small) to the gradient was not computed. This gives the lowest energy point on the crossing, at which there are two coordinates, the gradient difference and derivative coupling vectors (branching space), which lift the degeneracy. The remaining $3N - 8$ coordinates (intersection space) preserve the

---

(54) Herzberg, G.; Longuet-Higgins, H. C. *Discuss. Faraday Soc.* **1963**, *35*, 77−82.

(55) Druzhinin, S. I.; Demeter, A.; Galievsky, V. A.; Yoshihara, T.; Zachariasse, K. A. *J. Phys. Chem. A* **2003**, *107*, 8075−8085.

(56) Frisch, M. J.; et al. *Gaussian 03*, revision B.07; Gaussian, Inc.: Wallingford, CT, 2004.

(57) (a) Herhe, W. J.; Ditchfield, R.; Pople, J. A. *J. Chem. Phys.* **1972**, *56*, 2257−2261. (b) Harihan, P. C.; Pople, J. A. *Theor. Chim. Acta* **1973**, *28*, 213−222.

(58) Klene, M.; Robb, M. A.; Blancafort, L.; Frisch, M. J. *J. Chem. Phys.* **2003**, *119*, 713−728.

(59) Boggio-Pasqua, M.; Bearpark, M. J.; Klene, M.; Robb, M. A. *J. Chem. Phys.* **2004**, *120*, 7849−7860.

(60) Andersson, K.; et al. MOLCAS, Version 5; University of Lund, Sweden, 2000.

(61) (a) Celani, P.; Robb, M. A.; Garavelli, M.; Bernardi, F.; Olivucci, M. *Chem. Phys. Lett.* **1995**, *243*, 1−8. (b) Garavelli, M.; Celani, P.; Fato, M.; Bearpark, M. J.; Smith, B. R.; Olivucci, M.; Robb, M. A. *J. Phys. Chem. A* **1997**, *101*, 2023−2032.

Table 1. Relative Energies between the Structures in ABN at the CASSCF, RASSCF, and CASPT2 Levels (All Energies Are in kcal mol^{-1})

geometry	ΔE CASSCF	ΔE RASSCF[a]	ΔE CASPT2[b]	ΔE CASPT2[c]
S_1-LE	0	0	0	0
S_1-(T)ICT	25.2	16.0	*21.8*/15.7	*23.7*/16.6
S_2-(P)ICT	35.0	28.5	*13.4*/14.5	*18.6*/19.7
S_1-TS	33.5	19.8	*12.8*/16.3	*14.8*/19.0
S_1/S_2 CI	26.9	22.7	[*7.8,21.1*]/ [8.1,21.2][d]	[*18.2,19.0*]/ [15.5,19.2][d]
S_0/S_1 CI	4.4	−6.9	[−19.8,5.5]	[−7.6,−0.6]
S_1 CI-LE TS	20.7	6.1	*11.6*/14.3	*14.5*/14.6

[a] Results obtained from fully reoptimized structures at the RASSCF-(18,7+4+7)[2,2]/6-31G* level. [b] CASPT2 calculations performed with CASSCF(12,11)/6-31G* reference wave function at the CASSCF optimized geometries. All of the CASSCF calculations were performed using state-averaged 0.5/0.5 for S_1/S_2 states (state-averaging results over the three states are given in italics). Multi-state corrections were included in CASPT2 calculations only at conical intersection geometries. [c] Same calculations as in (b) but at RASSCF optimized geometries. [d] Energy differences with respect to LE for the two CASPT2 energies corresponding to the S_1 and S_2 states. The large difference between these two values shows that the two states are not degenerate anymore at the CASPT2 level.

degeneracy, which therefore persists over a wide range of molecular geometries. Decay can take place away from the minimum energy point on the crossing depending on the kinetic energy of the system. Sections of crossing seams were computed by minimizing the energy difference along the gradient difference vector only, at varying geometries in the intersection space.

VB structures have been determined exploiting the results of the computation of the second-order exchange density matrix P_{ij} and the diagonal elements of the electronic density matrix (see ref 62 for details). The elements of P_{ij} have a simple physical interpretation, which is related to the spin coupling between the electrons localized in the orbitals residing on the atoms *i* and *j*.[63] An illustration of the meaning of these matrix elements can be found in ref 62.

Results and Discussion

Mechanistic Overview. We begin with the discussion of the general features of the topology of the first two excited states that have come from our computations. We shall focus on the main mechanistic features that emerge and then return to a more detailed documentation of our results. The generic topological features of the computed potential energy surfaces are summarized in the "cartoons" shown in Figures 1 and 2.

The central mechanistic feature is concerned with the extended conical intersection hyperline between S_1 and S_2 shown in Figure 1 (and discussed earlier in relation to Scheme 3). The degeneracy-lifting coordinates X_1 and X_2 involve mainly skeletal deformations, neither torsion nor pyramidalization (i.e., pure torsion and pyramidalization do not lift the degeneracy). Thus, the S_1/S_2 degeneracy is preserved along the amino-group torsion (the shaded coordinate in Figure 1), which belongs to the intersection space. The "seam" of degeneracy, represented by the thick line between the points A and B, corresponds to the amino torsion coordinate (and pyramidalization). Point A (zero torsion) corresponds to the minimum on the crossing seam. At point B (90° torsion of the amino group), S_1/S_2 degeneracy remains and the total energy has increased (as shown by the gradient of color on the torsion axis).

The most important mechanistic ideas are associated with the fact that the local topology of the two potential energy surfaces associated with the S_1/S_2 conical intersection (shown in Figure 1 as two opposed conical surfaces) changes between geometry A and geometry B. At point A, the ICT state ($A^-{-}D^+$) has a minimum on S_2 at S_2-(P)ICT and the dot-dot LE state (A−D) has a minimum on S_1 at S_1-LE. We have also found a minimum corresponding to S_1-(R)ICT, but no S_1-(P)ICT minimum could be located. The S_2-LE structure shown in Figure 1 must exist at the position indicated, but not necessarily as a critical point or minimum that can be optimized. As we shall discuss subsequently, the S_1-(R)ICT structure has an electronic structure very similar to S_2-(P)ICT except that the C−C−N cyano angle is 122°. (There may be a S_1-(P)ICT with a linear C−C−N angle that would be a transition state; however, the S_1-(R)ICT structure is too high in energy to be mechanistically interesting.) In contrast, at point B (twisted amino group), the ICT state now has its minimum on S_1 at S_1-(T)ICT, whereas no potential energy minima were found for the LE state (shown as S_2-(T)-LE in Figure 1) on either S_2 or S_1. Thus, the ICT state has minima both (a) at zero torsional angles on S_2 at S_2-(P)ICT as well as on S_1 at S_1-(R)ICT and (b) at 90° torsional angle on S_1 at S_1-(T)ICT.

In Figure 2, we show another "cartoon" where the S_1 and S_2 potential energy surfaces have been represented in a space defined by one of the two branching coordinates (X_1 or X_2) and the reaction coordinate X_3 (i.e., mainly torsion). As introduced in relation to Scheme 4b, in this representation, the extended conical intersection hyperline appears as a "seam" in three dimensions (red line labeled CI). The same minima shown in Figure 1 also appear in this figure (apart from S_1-(R)ICT, which has been left deliberately). However, in this representation, the relationship between the reaction path and the conical intersection seam becomes clear. (We emphasize that Figure 2 is a simplified cartoon. It is correct only when the reaction coordinate excludes (i.e., is orthogonal to) the branching space coordinates. The real transition state, shown as S_1-TS in Figure 2, involves motions other than simple torsion.) The two minima on S_1, the dot-dot S_1-LE structure and the charge-transfer S_1-(T)ICT, are shown in Figure 2, in addition to the transition state (S_1-TS) connecting them. The ICT minimum on S_2, S_2-(P)ICT, is also shown together with the reaction path that leads to the minimum energy crossing on the seam. Thus, the reaction paths for ICT in DMABN following photoexcitation can be visualized in the cartoon corresponding to Figure 2. Two reaction pathways appear: (i) a nonadiabatic reaction path evolving on S_2 leading to the transient S_2-(P)ICT structure and then decaying at the minimum energy point on the CI (green curve), and (ii) an adiabatic reaction path on S_1 between S_1-LE and S_1-(T)ICT (blue curve). Thus, after photoexcitation, the system relaxes on S_2 to reach the S_2-(P)ICT minimum region. This minimum is shallow, and the crossing seam CI can easily be accessed. Depending on the extent of torsional or pyramidal vibrational motion, the $S_2 \rightarrow S_1$ internal conversion can occur anywhere along the crossing seam (i.e., at any twist angle of the amino group), and therefore can lead to the simultaneous formation of S_1-LE and S_1-(T)ICT (two green curves evolving on S_1 in Figure 2). We expect that the internal conversion directly to S_1-LE will be favored, because the minimum structure on the crossing seam is not twisted in S_2-(P)ICT. Decay at low torsion angles is

---

(62) Blancafort, L.; Celani, P.; Bearpark, M. J.; Robb, M. A. *Theor. Chem. Acc.* **2003**, *110*, 92−99.

(63) McWeeny, R.; Sutcliffe, B. T. *Molecular Quantum Mechanics*; Academic Press: New York, 1969; pp 148−170.

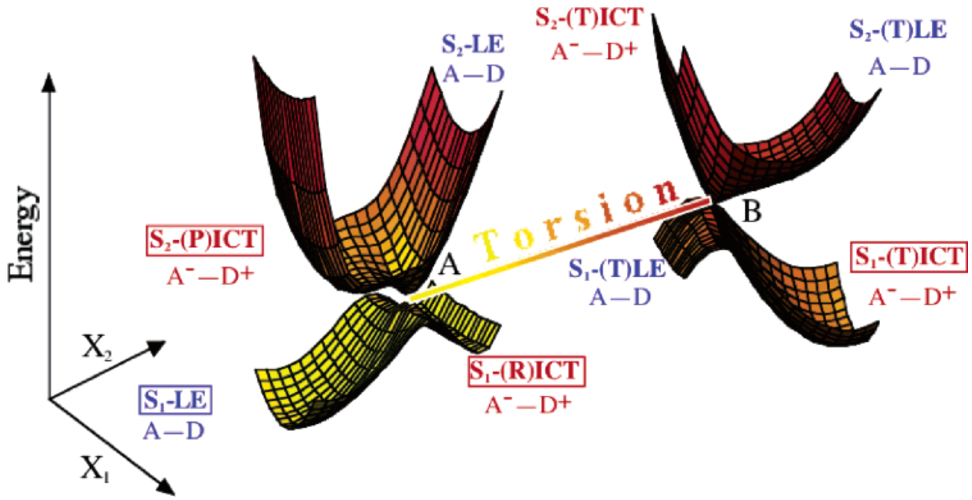

Figure 1. Schematic representation of the extended S_1/S_2 conical intersection in a four-dimensional space (see Scheme 3), including both the branching space (X_1, X_2) and the amino-group torsion (intersection space) as well as the energy. The torsional coordinate is represented by the shaded axis linking geometries A (zero torsion) and B (orthogonal amino group). The true optimized minima have been enclosed with a square box, while structures that must exist theoretically have been indicated simply with the VB label.

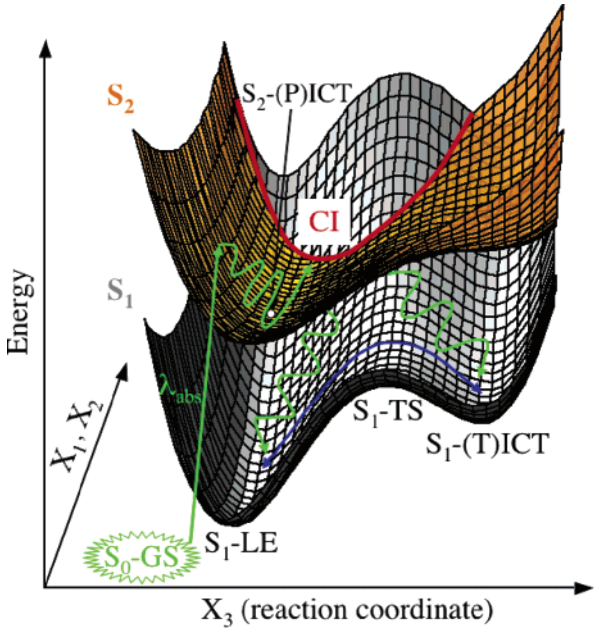

Figure 2. Schematic representation of the conical intersection between S_1 and S_2 in a space that includes one of the two branching space coordinates (X_1, X_2) and the reaction coordinate (mainly amino group torsion), and the energy. The green curve shows the nonadiabatic pathway. The blue curve shows the adiabatic pathway.

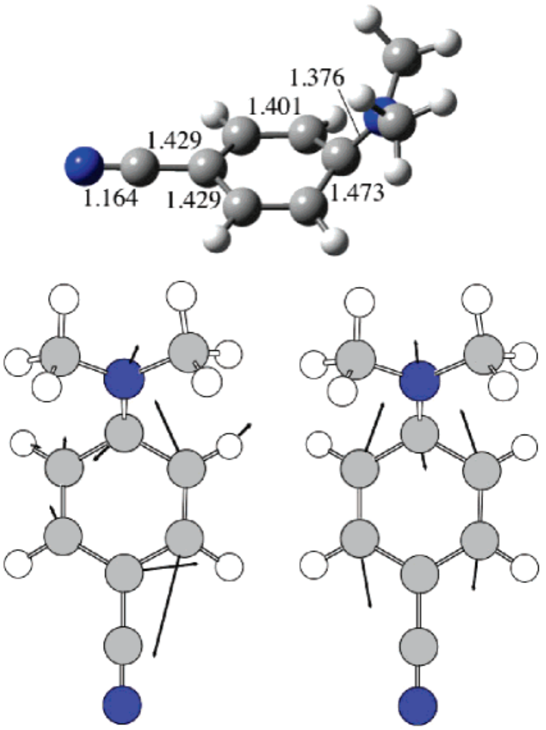

Figure 3. S_1/S_2 conical intersection in DMABN. Degeneracy-lifting coordinates: derivative coupling vector (left) and gradient difference vector (right). All bond lengths are in angstroms.

probably even more favored in solution because of the friction with the solvent. Thus, relaxation to S_1-LE is favored both energetically and dynamically. This could explain why all of the experimental evidence in solution points to S_1-LE as the sole precursor of ICT. The internal conversion should be followed by an adiabatic equilibration between S_1-LE and S_1-(T)ICT along the blue curve. The final populations of the two states depend on the relative energy and energy barriers, controlling the dual fluorescence.

Characterization of the Nonadabatic ICT Process Associated with Radiationless Decay from $L_a(S_2)$ to $L_b(S_1)$. The molecular structure of the lowest point on the S_1/S_2 conical intersection seam is displayed in Figure 3 together with the two degeneracy-lifting coordinates defining the branching space (derivative coupling and gradient difference vectors, see Figure S1 for ABN). These two coordinates correspond to X_1 and X_2 in Figure 1. The most important point to make is that the branching space does not involve either the amino group twist or the pyramidalization coordinates and thus the S_1/S_2 degeneracy will be preserved along the amino group torsion (Figure 1). Thus, the branching space is dominated by skeletal deformations of the phenyl ring coupled with the C−N stretch. A segment of the extended conical intersection seam is shown quantitatively in Figure 4 (see Figure S2 for ABN) for amino group torsion and pyramidalization of the ring carbon atom of the $CNMe_2$ group (there is also a slight pyramidalization of the

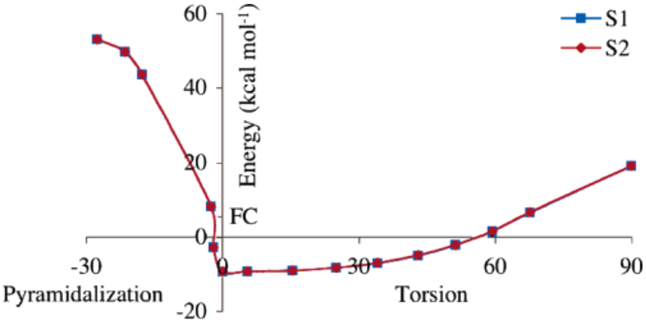

Figure 4. Crossing seam along the amino group twist and pyramidalization of the carbon atom carrying the dimethylamino group in DMABN. Angles are relative to the value at the CASSCF optimized conical intersection geometry. The origin is the optimized pyramidalized structure shown in Figure 3, and the zero energy corresponds to the optimized S_2-(P)ICT structure. The structure at −30° pyramidalization corresponds to the planar conical intersection structure. Franck−Condon (FC) energy on S_2 is 5.6 kcal mol^{-1} above S_2-(P)ICT.

dimethylamino group itself, which was taken into account). From this figure, it can be seen that the energy of the conical intersection seam at planar geometries (shown as −30 in Figure 4) is quite high and the low energy crossing region occurs along the torsional coordinate. The lowest energy path from the S_2-(P)ICT minimum involves pyramidalization. This feature was confirmed by an interpolated energy path calculation between S_2-(P)ICT and S_1/S_2 CI (Figure S3). A very small barrier of 0.15 kcal/mol was found (but no transition structure could be optimized).

The most important mechanistic point, which arises from Figure 4, is that the seam is energetically accessible for the complete range of torsional angles. Thus, $S_2 \rightarrow S_1$ nonradiative decay (internal conversion) can take place over the full range of torsion angles, depending on the vibrational energy in torsional coordinates following photoexcitation. It then follows that both the S_1-LE and the S_1-(T)ICT minima could be populated after internal conversion at the seam. This is in agreement with Fuβ interpretation of his observations: simultaneous formation of LE and TICT on S_1 in DMABN.[26] (Fuβ is the only researcher to have observed this phenomenon to date.) Finally, note that Fuβ has interpreted his experiments using a branching space consisting of torsion and pyramidalization of the amino nitrogen and this interpretation will need to be revisited because our computations suggest that the branching space includes only skeletal deformations. Note that Zilberg and Haas[37] suggested that the conical intersection is found along two coordinates: the Kekulé/anti-Kekulé mode and the quinoidization/anti-quinoidization mode. Although they did not optimize the conical intersection, their finding is in agreement with our calculation of the branching space.

A crucial point in our proposed mechanism is that, although no S_1-(P)ICT minimum could be located in ABN and DMABN, this minimum (when it exists) could be populated because the $S_2 \rightarrow S_1$ internal conversion does not need the amino group twist. For the same reasons, S_1-(R)ICT could be populated as those two structures are closely related as explained previously. There may be some systems for which the S_1-(R)ICT is lower in energy than S_1-(P)ICT (with S_1-(P)ICT possibly being a transition state between the two mirror images of S_1-(R)ICT) like in ABN and DMABN, but that is lower in energy than S_1-(T)ICT or at least accessible in energy.

From a mechanistic point of view, it is the potential surface topology that is important (Figures 1 and 2) and highly accurate energetics are not essential to obtain qualitative mechanistic information, which is the main target of these computations. Nevertheless, the electronic structures of the ICT state and the LE state are very different, and one might expect that dynamic electron correlation might change even the potential surface topology.[64] Accordingly, we have attempted to increase the confidence levels in our work by assessing the importance of the dynamic correlation.[64] The conical intersection has been reoptimized with the RASSCF method (in which one can include an important part of the dynamic electron correlation yet still reoptimize the geometry). As a further check, we have also computed CASPT2 energies at both CASSCF and RASSCF geometries. The results are displayed in Table 1. The CASPT2 S_1-S_2 CI energy gap is about 13 kcal mol^{-1} using the CASSCF optimized conical intersection geometry. This is reduced to between 0.8 and 3.7 kcal mol^{-1} at the RASSCF geometry. This highlights the importance of reoptimizing the structures with dynamic correlation included. However, the RASSCF and CASPT2 computations do show that the CASSCF results are qualitatively correct and give the main geometrical and topological features of the crossing (no twist, pyramidalization).

Characterization of S_1 Adiabatic ICT Reaction Path. The energetics for the adiabatic minimum energy path connecting the S_1 LE and (T)ICT minima for DMABN and ABN are summarized in Figure 5 together with the general shape of the conical intersection line. The reaction coordinate (which we shall document in the next section) is dominated by the amino group twist, but also involves the quinoid/anti-quinoid benzene ring skeletal deformations together with C−N stretching and the pyramidalization of the carbon atom in the $CN(Me)_2$ group. In DMABN, the energies associated with the S_1-LE and S_1-(T)ICT minima differ by 2.4 kcal mol^{-1} (in good agreement with the best coupled-cluster calculation of 3.9 kcal mol^{-1}),[39] and there is a 15.7 kcal mol^{-1} ICT→LE barrier. Thus, the ICT state could be populated after equilibration, and this effect will be enhanced in a polar solvent, which would stabilize this state further. In ABN, the S_1-LE/S_1-(T)ICT energy difference is 25.2 kcal mol^{-1}, and the ICT→LE barrier is reduced to 8.3 kcal mol^{-1}. Therefore, the ABN equilibrium is strongly displaced toward the LE state and population of S_1-(T)ICT would not be detectable.

To test the effects of dynamic electron correlation, RASSCF and CASPT2 computations have been carried out for ABN (see Figure 5 and Table 1). The S_1-LE/ S_1-(T)ICT energy difference and the ICT→LE barrier are reduced to 16.0 and 3.8 kcal mol^{-1}, respectively. These results reinforce the fact that S_1-TICT is not populated in ABN. Note that considering the effects of including dynamic correlation, the CASSCF ICT→LE barrier in DMABN is probably overestimated. Referring to Table 1, one observes that the RASSCF energetics are comparable to the CASPT2 when the RASSCF geometries are used in the CASPT2 computations. Note that, although energetics are affected by dynamic correlation, the global topology of the potential energy surface is not changed.

Geometry, VB Structures of the LE and ICT Intramolecular Charge-Transfer Minima. We now turn to a discussion of the geometry of the various critical points together with an analysis of the wave function using VB notation. It is these

---

(64) Borden, W. T.; Davidson, E. R. *Acc. Chem. Res.* **1996**, *29*, 67−75.

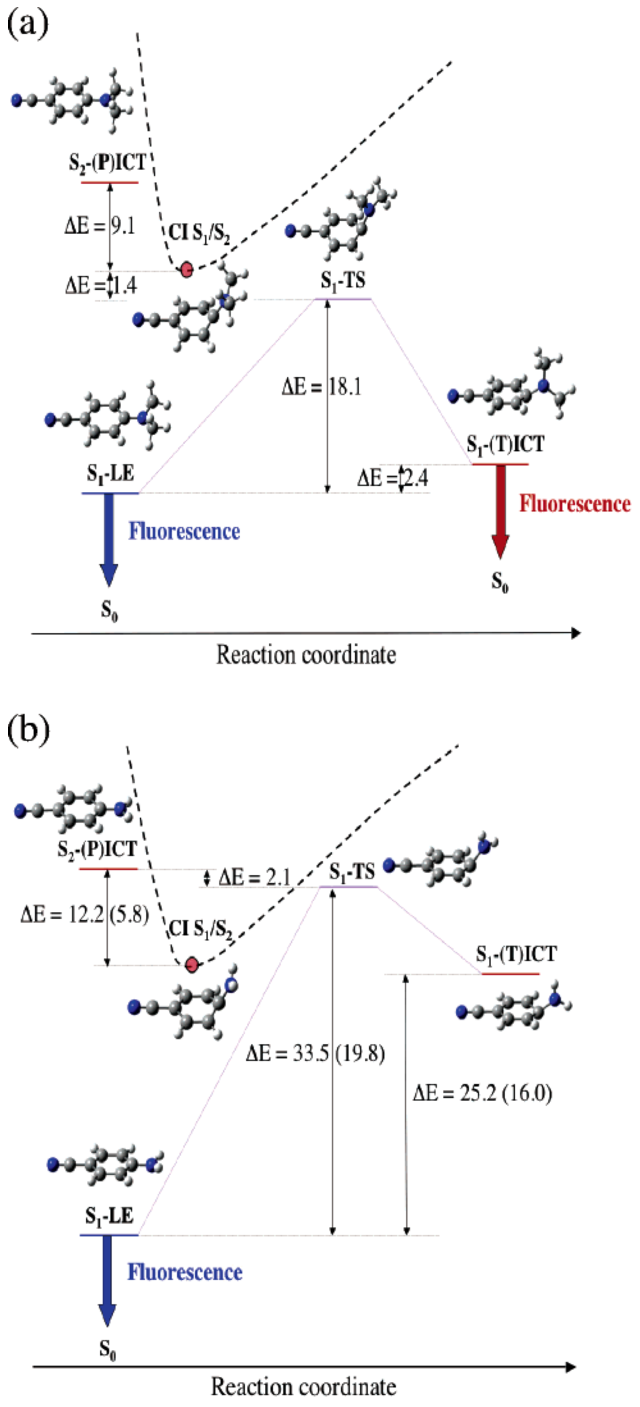

Figure 5. Schematic potential energy profiles for (a) DMABN and (b) ABN. RASSCF energetics are given in parentheses. Energetics are in kcal mol^{-1}.

structural and electronic descriptions of the various minima that lie at the heart of the TICT controversy. In Figure 6 (Figure S4 for ABN), we show the geometries of the various minima optimized on S_0, S_1, and S_2 together with the VB structures derived from the analysis of the corresponding wave function, which are shown in Figure 7 (Figure S5 for ABN). Figure S6 displays the transition state structure along with the transition vector in ABN. By comparing the molecular geometry for the LE and TICT critical points in Figure 6, the adiabatic ICT reaction path can be characterized. Clearly, the S_1 adiabatic reaction coordinate is dominated by the amino group twist, but also involves the quinoidization skeleton deformations of the benzene ring together with C−N stretching and the pyramidalization of the $CN(Me)_2$ group involving both pyramidalization of the carbon and nitrogen atoms in anti position.

We begin with a discussion of the electronic (VB) structures of the various critical points for DMABN (shown in Figure 6 and derived from the data in Figure 7). The electronic structure of the ground state (denoted S_0-GS) corresponds to an in-phase combination of the two Kekulé structures (see Scheme 1). It is clear that this covalent nature (dot-dot) is retained in the S_1-LE state (similar dipole moment). On inspection of Figure 7, one can see that the occupancies of the orbitals for the S_0-GS and S_1-LE are similar, and it is the bonding that is different (because of the anti-Kekulé benzene moiety in S_1-LE). It is also clear from Figure 6 that the S_2-(P)ICT, S_1-(R)ICT, and the S_1-(T)ICT minima have similar zwitterionic character with (partial) positive charge on the nitrogen and a phenyl quinoidal radical anion resonance structure giving rise to a large dipole moment (note that the dipole moments for LE and TICT are lower than the experimental ones because the dipole moments were measured in a polar solvent). The major difference between S_2-(P)ICT and S_1-(T)ICT is the magnitude of the charge transfer (fraction of electron transferred), being slightly greater in TICT as expected (see Figure 7). The similar electronic (VB) structures for S_2-(P)ICT, S_1-(R)ICT, and S_1-(T)ICT are expected because these states are diabatically linked across the conical intersection seam as shown in Scheme 2, and Figures 1 and 2. In the ICT minimum with a bent cyano group S_1-(R)ICT, the negative charge resides on the cyano nitrogen atom. Because of the larger distance between the charges, S_1-(R)ICT has the largest dipole moment, although S_1-(T)ICT displays the highest charge transfer (a net charge of +1 is found on the amino nitrogen atom). However, S_1-(R)ICT lies 33 kcal mol^{-1} higher in energy than S_1-LE in DMABN, so this species is not important mechanistically.

We now discuss the relaxed geometries shown in Figure 6. As one might expect, these relaxed geometries reflect the electronic (VB) structures just discussed (e.g., the increased bond lengths in the phenyl ring on comparing S_0-GS and S_1-LE reflect the Kekulé phenyl ring in S_0-GS versus anti-Kekulé nature of S_1-LE). We shall try and emphasize this point in our discussion. Further, we also want to quantify, for example, the extent of the phenyl amino coupling in the ICT species.

Our optimized structure for S_0-GS has a pyramidal amino group in agreement with X-ray crystal structures,[65] microwave and high-resolution spectroscopy,[66] as well as results reported from previous calculations.[32,36] This pyramidalization corresponds to an inversion of the amino group and can be quantified by measuring the pyramidalization angle θ as defined in ref 36. We found $\theta = 25.7°$ (43.0° for ABN) slightly larger than the experimental value $\theta = 11.9°$[65] and 15°[66] (34° for ABN[65]). The computed bond lengths are slightly larger than the X-ray data[65] with a standard error of 0.015 Å.

Our optimized geometry for the S_1-LE minimum is untwisted and has a pyramidal geometry with the nitrogen and the carbon atoms of the dimethyl-amino group slightly out of plane, like in S_0-GS. We found $\theta = 21.0°$ (40° and 28° for ABN at

---

[65] Heine, A.; Herbst-Irmer, R.; Stalke, D.; Kühnle, W.; Zachariasse, K. A. *Acta Crystallogr.* **1994**, *B50*, 363−373.

[66] Kajimoto, O.; Yokoyama, H.; Ooshima, Y.; Endo, Y. *Chem. Phys. Lett.* **1991**, *179*, 455−459.

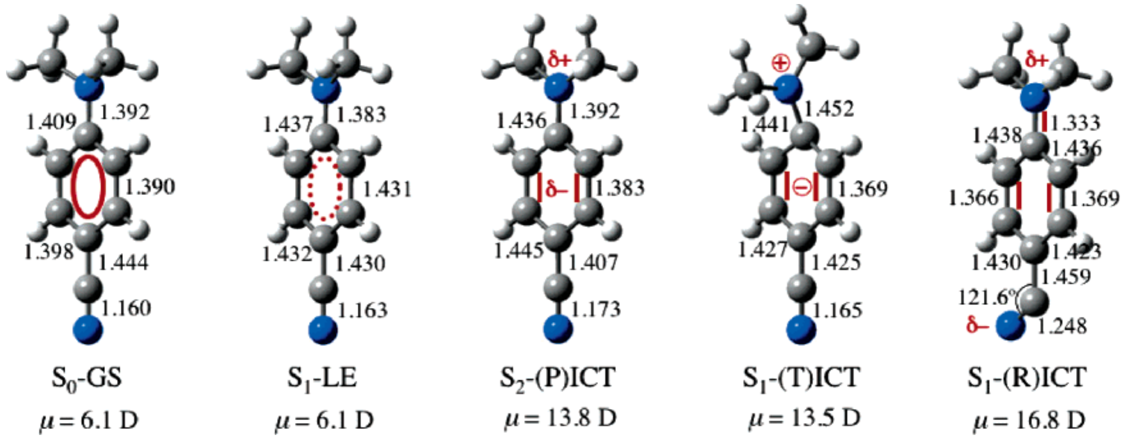

Figure 6. Geometries and electronic structures (in red) of the ground state, LE, PICT, TICT, and RICT minima in DMABN. All bond lengths are in angstroms.

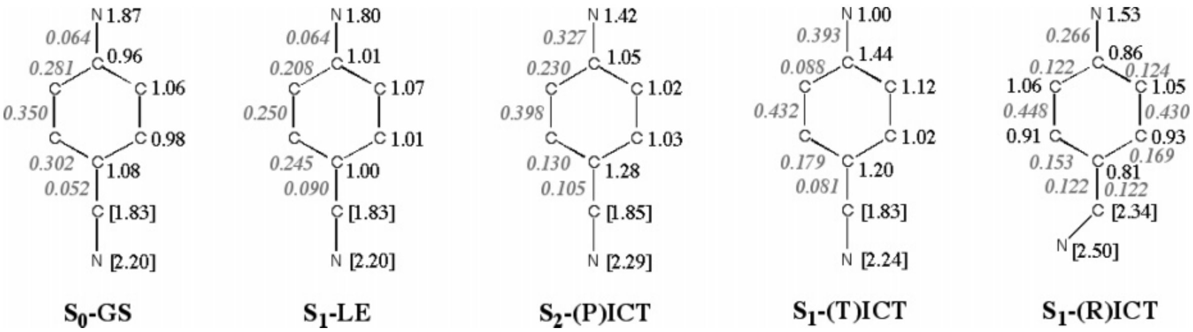

Figure 7. Values of the second-order exchange density matrix (in italic gray) and the one-electron density matrix (in black) in DMABN structures. Values in brackets refer to the sum of the in- and out-of-plane components.

CASSCF and RASSCF levels, respectively) in fairly good agreement with 25.0° obtained with minimal CASSCF calculations.[36] The phenyl CC bonds are expanded as expected from the out-of-phase combination of two Kekuké structures. Zachariasse[67] observed an expansion of the benzene ring of ABN (with the two central CC bonds increasing less than the other four CC bonds) and a contraction of the CN amino bond upon excitation to S_1. This is in very good agreement with our RASSCF calculations (see Figure S4). Note that the amino nitrogen is slightly out of the phenyl plane by ca. 2° and at opposite side (anti) with the methyl groups. This does not seem to be due to numerical inaccuracy as the phenomenon is observed in ABN as well and persists when dynamic correlation is included with RASSCF. This is also observed in S_0-GS. These geometrical effects have been observed experimentally from rotationally resolved electronic spectroscopy of ABN.[67]

There is disagreement in the literature about the structure of the S_1-LE minimum. Rotationally resolved electronic spectroscopy[67] predicts a pyramidal LE minimum for ABN. Experimental infrared band intensities[68] and picosecond time-resolved resonance Raman and transient absorption spectroscopy[21] predict a planar conformation of the LE state, in agreement with previous CASSCF calculations,[28,69] and semiempirical studies.[40,46] However, recent experiment information extracted from the vibronic structure of the $S_1 \leftarrow S_0$ band[70] and a number of computations support a twisted structure.[32,39,71] Finally, Dreyer and Kummrow[36] found two LE states both of planar and of pyramidal structure at the CASSCF level.

We now move to the S_1-(T)ICT structure. Our calculations show that the CN(Me)$_2$ group is pyramidalized as well as being twisted so that the symmetry is C_s. Both the nitrogen of the amino group and the carbon of the phenyl carrying that group are out-of-plane with respect to the phenyl ring. The nitrogen is out-of-plane by ca. 14° (18° for ABN at both CASSCF and RASSCF levels), while the carbon is out-of-plane by ca. 10° (11° for ABN at both CASSCF and RASSCF levels) but in anti position. The twisted S_1 minimum was previously found to have C_{2v} symmetry.[29,36,38] Our result agrees with recent calculations from Köhn and Hättig,[39] while picosecond time-resolved resonance Raman spectroscopy[21] suggests the pyramidal character of the dimethylamino group in S_1-(T)ICT.

In S_1-(T)ICT structure, the N-phenyl bond length is enlarged by 0.06 Å with respect to the ground state. (This is in agreement with previous CASSCF calculations[36] and CC2 calculations.[39]) In contrast, the N-phenyl bond length in S_2-(P)ICT and S_1-(R)ICT is much shorter than that in S_1-(T)ICT. This leads us to the central mechanistic question concerned with the coupling between the amino group and the benzene ring. In Figure 7, it can be seen that the coupling between the nitrogen lone pair and the phenyl ring is large for the ICT structures (0.327 in (P)-ICT, 0.266 in (R)-ICT, and 0.393 in (T)ICT) as

---

(67) Berden, G.; van Rooy, J.; Meerts, W. L.; Zachariasse, K. A. *Chem. Phys. Lett.* **1997**, *278*, 373−379.

(68) Kummrow, A.; Dreyer, J.; Chudoba, C.; Stenger, J.; Theodorus, E.; Nibbering, E. T. J.; Elsaesser, T. *J. Chin. Chem. Soc.* **2000**, *47*, 721−728.

(69) Chudoba, C.; Kummrow, A.; Dreyer, J.; Stenger, J.; Nibbering, E. T. J.; Elsaesser, T.; Zachariasse, K. A. *Chem. Phys. Lett.* **1999**, *309*, 357−363.

(70) Saigusa, H.; Miyakoshi, N.; Mukai, C.; Fukagawa, T.; Kohtani, S.; Nakagaki, R.; Gordon, R. *J. Chem. Phys.* **2003**, *119*, 5414−5422.

(71) Scholes, G. D.; Phillips, D.; Gould, I. R. *Chem. Phys. Lett.* **1997**, *266*, 521−526.

compared to dot-dot structures (0.06 in S_0-GS and S_1-LE). This is a characteristic property of the ICT state. However, because of the zero overlap of the orbitals involved in S_1-(T)ICT, the electronic stabilization from this effect is zero. On the other hand, because of the strong orbital overlap in S_2-(P)ICT (and S_1-(R)ICT)), the attractive spin-exchange interaction is effective and is manifested in the shorter N-phenyl bond length. This is in agreement with Zachariasse's claim that the amino group is strongly coupled to the phenyl moiety.[15,16]

The phenyl ring of S_1-(T)ICT exhibits a quinoidal geometry, even when dynamic correlation effects are included (see RASSCF structure in Figure S4). It has been suggested that such a quinoidal structure is incompatible with a twisted structure.[37] Nonetheless, this effect has now been observed in a number of accurate calculations.[29,36,38,39] The computations[37] suggesting a planar ICT state used a rather restricted active space.

Thermally Activated Internal Conversion from the Locally Excited-State S_1-LE. In this section, we discuss the possible nonradiative decay channel by internal conversion to the ground state from S_1. Zachariasse and co-workers[55] have observed that the fluorescence decay time and quantum yield strongly decrease with increasing temperature in DMABN and ABN in an alkane solvent. They have established that DMABN and ABN undergo efficient thermally activated internal conversion (IC). Upon increasing the temperature for DMABN in *n*-hexadecane from 18 to 287 °C, the IC yield increases from 0.04 to 0.95. This occurs at the expense of intersystem crossing (ISC) and fluorescence quantum yield. Thus, IC replaces ISC as the dominating deactivation pathway of the first excited singlet state S_1 at temperatures higher than 125 °C. The IC activation energies have similar values for both DMABN (7.5 kcal mol^{-1}) and ABN (8.3 kcal mol^{-1}). Because ICT is not present in alkane solvents for these systems, the thermally activated IC process is not mechanistically related to ICT. Nonetheless, this channel should be taken into account as excitation energies to the higher S_2 excited state would leave the system with sufficient energy to access such a deactivation channel.

Figure 8 displays the structure for the S_0/S_1 CI corresponding to the funnel for the thermally activated IC, as well as the transition state, which links this funnel to the S_1-LE minimum (see Figure S7 for ABN). The funnel lies less than 3 kcal mol^{-1} above the S_1-LE minimum. Because the distortion needed to take the system from the S_1-LE minimum to the funnel (mainly pyramidalization of the ring carbon atom carrying NMe_2 and wagging of the amino nitrogen) is strongly unfavorable energetically in the ground state, the energy gap between S_1 and S_0 is rapidly reduced along this coordinate, opening up an IC deactivation channel. As pointed out in ref 55, the measured IC activation energy corresponds to the barrier that has to be overcome to bring the system to the S_0/S_1 CI. The CASSCF IC potential energy barrier is 19.9 kcal mol^{-1} for DMABN and 20.7 kcal mol^{-1} for ABN. CASPT2 calculations at the conical intersection geometry for ABN give an S_0-S_1 energy gap of about 20 kcal mol^{-1}. Those results show that both structures and energetics are inaccurate at CASSCF. Accordingly, we performed RASSCF optimizations for ABN. The structures are presented in Figure S6. The IC barrier is now reduced to 6.1 kcal mol^{-1}, in much better agreement with the experimental result (8.3 kcal mol^{-1}).[55] Moreover, the CASPT2 S_0-S_1 energy gap computed at RASSCF conical intersection geometry decreases to 7 kcal mol^{-1} (see Table 1). Note that the IC barrier decreases to about 14 kcal mol^{-1} with CASPT2 computed at both the CASSCF and the RASSCF geometries.

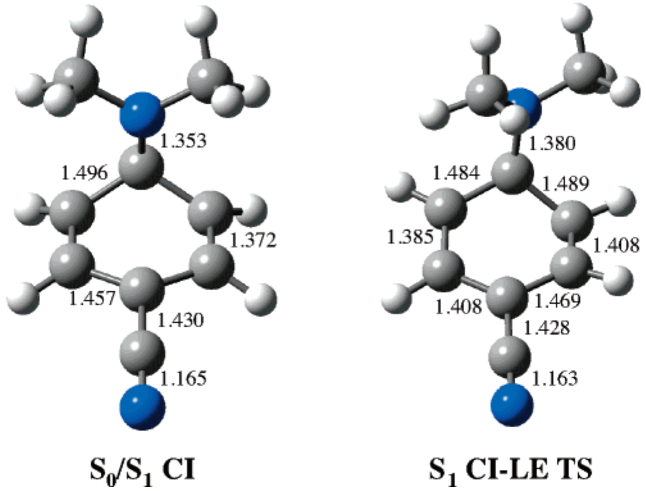

Figure 8. Geometries of the S_0/S_1 conical intersection in DMABN and the transition state on S_1 linking that crossing to S_1-LE. All bond lengths are in angstroms.

Conclusion

This study stands out among a long list of theoretical works for being the first to have accurately characterized the $S_2 \rightarrow S_1$ deactivation channel and the adiabatic S_1 equilibration path between the LE and ICT states in 4-aminobenzonitriles. The level of calculation used allows one to describe both states with a good level of confidence thanks to the inclusion of dynamic correlation effects combined with geometry optimizations. We believe that the results just presented clarify some aspects of the controversy associated with electron donor/acceptor TICT processes. The mechanism is remarkably simple. After excitation to the S_2 state, the system relaxes quickly to the shallow S_2-(P)ICT minimum (see IRC calculation in Figure S8). No significant barrier occurs between S_2-(P)ICT and the optimized S_1/S_2 CI (see Figure S3). Because of the extended conical intersection seam, ultrafast nonradiative $S_2 \rightarrow S_1$ decay can take place at various torsion angles of the dimethyl-amino group leading to either S_1-LE or S_1-(T)ICT geometries. Experimentally, the ultrafast decay through the S_1/S_2 CI leads to both LE and TICT simultaneously.[26] The branching at the CI favors the formation of the LE state because the lowest energy point on the crossing seam is not twisted. Equilibration can then occur on S_1, so the dual fluorescence is controlled by the S_1-LE and S_1-(T)ICT adiabatic reaction path. In ABN, because the equilibrium is displaced toward the LE minimum, the S_1-(T)ICT minimum is not populated, and fluorescence occurs only from the S_1-LE state. This result was reinforced by RASSCF calculations (reoptimizing the geometry) including dynamic correlation. Moreover, the $S_1 \rightarrow S_0$ deactivation channel accessible from the S_1-LE state was also identified.

Finally, a discussion about the observation of dual fluorescence in planar rigidized CT systems[24,25] is necessary. This phenomenon is not inconsistent with our proposed mechanism for ICT. Because pyramidalization is not constrained in those systems, the conical intersection will still be accessible along this coordinate. Although in the case of DMABN we found the ICT emitting species to be the S_1-(T)ICT state, we believe that the ICT S_1 minimum structure will depend on the system (type of compounds and substituents) and the environment (crystal or solution, solvent, ...). In the case of the observations on DIABN, the experiment was realized in a solid phase.[23,72] Considering DIABN molecules are present as pairs in a T-shaped configuration[72] and therefore the amino group torsion should not be hindered, it would be interesting to investigate the potential energy surfaces of such a system to understand why emission is attributed to a planar ICT. It seems there is a strong substituent effect upon replacing methyl by isopropyl groups. Further, in planar rigidized systems NTC6[24] or FPP,[25] the S_1 ICT minimum is expected to be planar and not twisted because the torsion of the amino group is sterically hindered. Thus, the ICT emitting species is a S_1-(P)ICT minimum (not S_2-(P)ICT which exists in both dual and nondual fluorescent systems). Note that Köhn and Hättig[39] suggest that NTC6 may still be able to twist in its ICT state and that data in ref 24 do not necessarily exclude a TICT mechanism. This conjecture has not been substantiated with any data, and calculations on these rigidized dual-fluorescent species are therefore necessary. An important point in our mechanism is that it does not exclude the S_1-(P)ICT mechanism because the $S_2 \rightarrow S_1$ internal conversion does not need the amino group twist. Finally, we should note that the role of the solvent in ICT mechanism is very important for the adiabatic equilibration and has not been included in this study. Nevertheless, we expect the solvent to affect mainly the energetics and not the topology of the potential surfaces.

Acknowledgment. This work has been supported by DGSIC of the Ministerio de Educación y Ciencia, (project no. BQU2002-04029-C02-02), by CIRIT of the Generalitat de Catalunya (grant 2001SGR-00315), and by EPSRC UK (grant GR/S94704/01). We would like to thank Professor Klaas Zachariasse for an extended e-mail discussion, which helped us to improve our original manuscript.

Supporting Information Available: Cartesian coordinates and energies of the optimized CASSCF and RASSCF structures. Figure S1 shows S_1/S_2 CI in ABN along with the branching space. Figure S2 shows the extended crossing seam in ABN. Figure S3 gives the energy path between S_2-(P)ICT and CI. Figure S4 displays the geometries and electronic structures for ABN. Figure S5 gives the VB structures in ABN. Figure S6 shows the transition state connecting S_1-LE and S_1-(T)ICT along with the transition vector. Figure S7 displays the S_0/S_1 CI and the transition state linking this funnel to S_1-LE in ABN. Figure S8 shows the IRC calculation from the Franck−Condon region in ABN. Complete refs 56 and 60. This material is available free of charge via the Internet at http://pubs.acs.org.

JA042413W

---

(72) Druzhinin, S. I.; Demeter, A.; Zachariasse, K. A. *Chem. Phys. Lett.* **2001**, *347*, 421−428.